Canadian Metallurgical Quarterly, Vol 45, No 4 pp 433-440, 2006

CYCLIC DAMAGE CHARACTERIZATION OF AN OFF-AXIS UNIDIRECTIONAL GRAPHITE BISMALEIMIDE COMPOSITE

K.J. CAIN, G. GLINKA and A. PLUMTREE

University of Waterloo, Waterloo, Ontario, Canada

(*Received in revised form May, 2006*)

Abstract — Cyclic tension-tension testing was performed on an off-axis (10°) unidirectional graphite bismaleimide (BMI) composite to determine the effect of the matrix dominant properties on the fatigue behaviour of the material. Rosette strain gauges mounted in the major directions were used to monitor cyclic stresses and strains while acetate replicas of surface cracks were taken as the number of cycles increased allowing a correlation of the stress-strain response with the accompanying cracking mechanisms to be established. Initial rapid crack nucleation and modulus degradation in the first 10% of life were followed by crack coalescence and steady state growth in the bulk material. Final fracture ensued from the development of coalesced matrix shear cracks parallel to the fibres. Comparing the amount of cracked area with modulus degradation, the decrease in shear modulus was found to be a more sensitive and practical parameter to represent fatigue damage evolution.

Résumé — On a effectué des essais cycliques tension-tension sur un composite excentré (10°), unidirectionnel, en graphite et bismaléimide (BMI) afin de déterminer l'effet des propriétés dominantes de la matrice sur la tenue en fatigue du matériau. On a utilisé des jauges de contraintes en rosette montées dans les directions principales pour observer les contraintes et les déformations cycliques tout en prenant des répliques en acétate des fissures de surface à mesure que le nombre de cycles augmentait, permettant d'établir une corrélation entre la réponse de contrainte-déformation et les mécanismes de fissurage qui l'accompagne. La nucléation initiale et rapide de fissure et la dégradation du module d'élasticité dans le premier 10% de vie étaient suivies par la coalescence de fissure et la croissance en régime permanent dans le matériau en vrac. La rupture finale a résulté du développement des fissures coalescées parallèles aux fibres, par cisaillement de la matrice. En comparant la superficie fissurée avec la dégradation du module d'élasticité, on a trouvé que la diminution du module de cisaillement était un paramètre plus sensible et plus pratique pour représenter l'évolution de l'endommagement par fatigue.

INTRODUCTION

With the increase in use of advanced composites in the aerospace and other manufacturing industries, more extensive studies on their strength and failure prediction are required. Long fibre composites are heterogeneous and, unlike more traditional isotropic materials, have different material properties in different directions. This results in crack growth in preferred directions. From the onset of loading, cracking may be widespread [1,2].

Laminated composites are generally composed of a series of thin unidirectional plies arranged in definite orientations that form cross-plies and quasi-isotropic laminates. As a result, studies on the fatigue of composites have concentrated mainly on multi-ply lay-ups [3-9] where delamination between the plies plays a vital role [3,10]. However, it is important to understand how damage evolves in an individual ply in order to form a basis for cyclic damage evolution in a multidirectional laminate. In an off-axis unidirectional composite, progressive matrix cracking and debonding can be studied without the complication of delamination. Testing an off-axis unidirectional composite has the additional advantage of experiencing little non-progressive fibre damage [11].

The current study considers the cyclic tension-tension testing of a unidirectional 10° off-axis graphite bismaleimide (BMI) composite. At this orientation, progressive fatigue damage occurs by matrix shear [12]. Damage evolution is modelled employing decreases in a fatigue modulus as well as changes in a cracked area. The intent of this work is to define an optimum parameter that expresses progressive matrix damage during cycling.

DAMAGE PARAMETERS

Off-axis composites loaded in cyclic tension develop damage in the form of microcracks in the matrix and along the fibre-

matrix interface parallel to the fibres (1-direction, see Figure 1). During cyclic loading, matrix cracks appear as early as the first cycle [13]. Applying damage mechanics, the area of these cracks can be summed to give the total cracked area allowing damage to be expressed [14] by

$$D = \frac{A_D}{A_o} \tag{1}$$

where A_D is the effective damaged area which may be larger than that observed because of accompanying stress concentrations and A_o is the total area of a representative volume element.

Through microscopic observation, it can be shown that the dominant cracking mechanism is matrix debonding in the fibre direction and is the same mechanism seen in quasi-static tests [15]. These cracks are generally in the 1 - 3 plane (Figure 1) and grow under the influence of shear stress, τ_{12}.

Modulus degradation has gained attention for *in situ* measurements in composites because of its sensitivity and monitoring ease [16-19]. Modulus-based damage can be derived from Equation 1 using the concept of effective stress and the principle of strain equivalence [20,21] giving

$$D = 1 - \frac{E}{E_o} \tag{2}$$

where E_o and E are the initial (N=1) and apparent elastic moduli (N>1), respectively with N being the cycle number. Here, the fatigue modulus is used, defined by the slope of a line connecting the origin of a stress-strain hysteresis loop to the maximum stress for any given cycle (N) [19] shown in Figure 2. Since the dominant damage mechanism which causes the final failure of a 10° fibre composite is matrix shear cracking parallel to the fibres [15], the damage due to shear modulus degradation can be monitored according to

$$D_{12} = 1 - \frac{G_{12}}{G_{12o}} \tag{3}$$

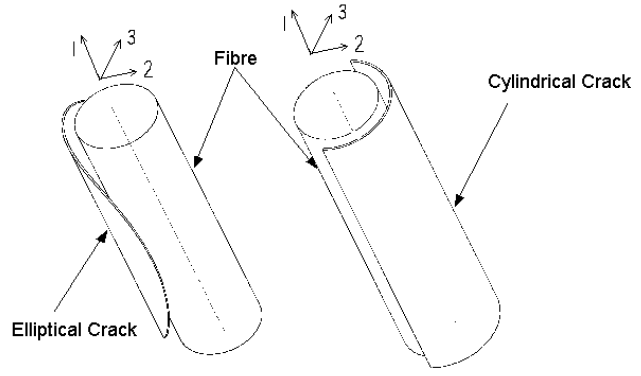

Fig. 1. Schematic of a small crack (elliptical) and a large crack (cylindrical) in the matrix around a fibre. Cracked areas are projected in the 1 - 3 plane for analysis.

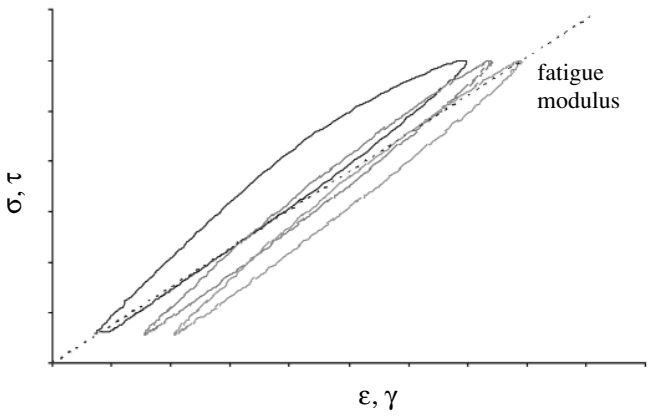

Fig.2. Definition of fatigue modulus.

where D_{12} is the damage in the shear plane, G_{12} is the apparent or fatigue shear modulus and G_{12o} is the initial shear modulus.

EXPERIMENTAL PROCEDURE

Fatigue specimens were prepared from 300 mm wide, 300 mm long and 2.8 mm thick unidirectional composite plates consisting of 58% volume fraction Hercules IM-6 graphite fibres in Narmco 5245C (Cytec) BMI resin matrix. The properties of the fibre and matrix are given in Table I [22,23] and those of the resulting composite are given in Table II [15,23]. All the specimens were approximately 250 mm long, 15 mm wide and 2.8 mm thick and cut so that the fibres were 10° off-axis. On loading, these long specimens experienced minimal in-plane bending according to measurements taken from extra rosette strain gauges mounted on the edges and tops of initial specimens. For most tests, rectangular aluminum tabs (50×15×2 mm) were attached to the ends of the specimen using an epoxy adhesive to prevent any damage caused by the test rig grips. Tapered tabs were also used for some companion tests. However, the results were the same.

During sample preparation and handling, care was taken to ensure minimal damage of the specimens. The machined edges of each specimen were smoothed with a dry 1200 Angstrom grit silicon carbide paper. Those areas where acetate replicas were to be placed were more finely polished with a slurry of 0.3 μm alumina powder in distilled water. On testing, the acetate replicas, using very thin SPI acetate tape softened with acetone, were taken immediately after recording the relevant stress-strain response. Once dried, they were mounted and sputter coated with a 4000 nm gold film for examination in a JEOL JSM-840 scanning electron microscope (SEM).

Cyclic testing was performed under load control with a stress ratio, R, of 0.1 using an Instron servo-hydraulic test machine equipped with mechanical self-tightening grips and a 156 kN load cell. Data were acquired from the load cell and rosette strain gauges mounted on the specimen surface. The

Table I - Mechanical properties of Hercules IM-6 graphite fibres (polyacrylonitrile (PAN) precursors based) and Narmco (Cytec) 5245C an epoxy modified bismaleimide resin [22,23]

Properties	Hercules IM-6 graphite fibre	Narmco (Cytec) 5245C resin
Tensile modulus (GPa)	296	3.3
Ultimate tensile strength (MPa)	4800	84
Ultimate strain (%)	1.74	1.25
Diameter (μm)	7-8	-
Strain energy release rate (J/mm^2)	-	67

Table II – Mechanical properties of a graphite (Hercules IM-6) BMI (Narmco 5245C) unidirectional lamina with a 58% fibre volume fraction [15,23]

Properties	Longitudinal 0°	Off-axis 10°	Transverse 90°
Tensile modulus (GPa)	173	94	8.5
Ultimate tensile strength (MPa)	2610	449	60.0
Ultimate strain (%)	1.50	-	0.72

strain gauges were stacked 0°/45°/90° rosette gauges manufactured by Showa Measurements Company Limited. At least 2 rosettes were attached to each specimen to duplicate and verify the strain readings taken throughout each test. All specimens were cycled at 10 Hz for at least a million cycles or to failure. However, the frequency was reduced to 1 Hz when the stress-strain data were being recorded. Temperature measurements indicated that negligible specimen heating occurred during cycling.

EXPERIMENTAL RESULTS

Cyclic Tests

Preliminary tensile test results on the off-axis graphite BMI composite gave a mean failure stress of 449 MPa with a standard deviation of 44.3 MPa [15]. The measured longitudinal and transverse moduli were in agreement with theoretical values given in Table II. These data formed the base for assessing changes in mechanical properties throughout the cyclic tests.

The fatigue specimens were cycled at constant maximum load levels and the results were compiled to form the stress-life curve shown in Figure 3. Runouts of one or more million cycles occurred for several specimens subjected to maximum stresses below 60% ultimate tensile strength. The equation of the S-N line was

$$\sigma_{\max} = 390 \times \left(N_f\right)^{-0.06} \tag{4}$$

The shallow Basquin slope of -0.06 is in agreement with Awerbuch and Hahn [24] for a similar composite.

Cyclic stress-strain hysteresis loops in the different material directions were recorded throughout the life of each specimen. Representative loops for a typical specimen are shown for the loading (Figure 4), longitudinal or fibre (Figure 5), transverse (Figure 6) and shear (Figure 7) directions, respectively.

A common observation was the progressive displacement of the hysteresis loops along the strain axis during cycling. This phenomenon, known as strain ratcheting, is clearly seen in Figures 6 and 7 for the transverse and shear directions. By contrast, the hysteresis loops for the loading and longitudinal directions (Figures 4 and 5) showed much smaller changes in permanent strain.

A large amount of strain ratcheting observed in the transverse loading direction (Figure 6) that took place during the early stages of life quickly saturated. However, the shear stress-strain loops (Figure 7) showed larger and more clearly

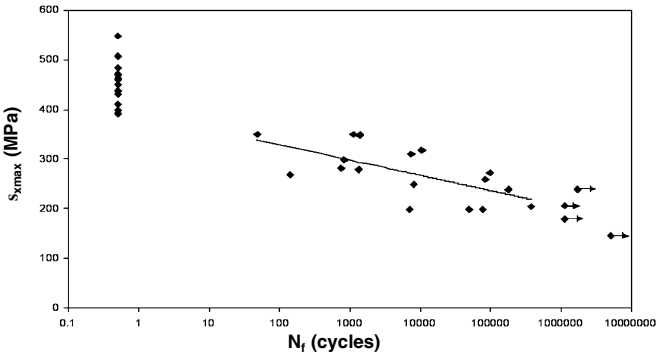

Fig. 3. Stress-life curve for 10° off-axis graphite BMI loaded in cyclic tension with R=0.1.

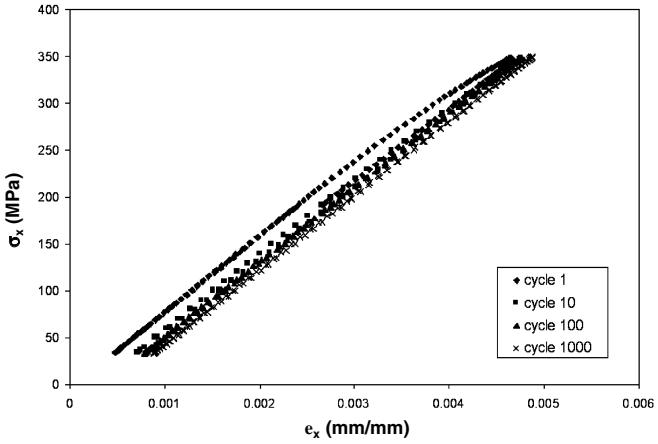

Fig. 4. Stress-strain curve for 10° off-axis graphite BMI in the loading (x) direction. σ_{max}=350 MPa, N_f=1158.

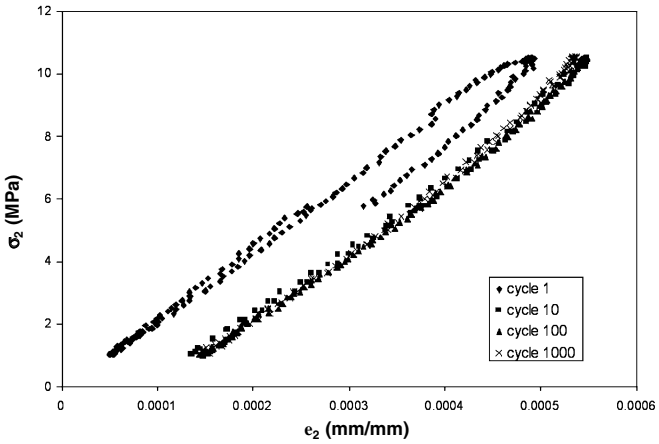

Fig. 6. Stress-strain curve for 10° off-axis graphite BMI in the transverse (2) direction. σ_{max}=350 MPa, N_f=1158.

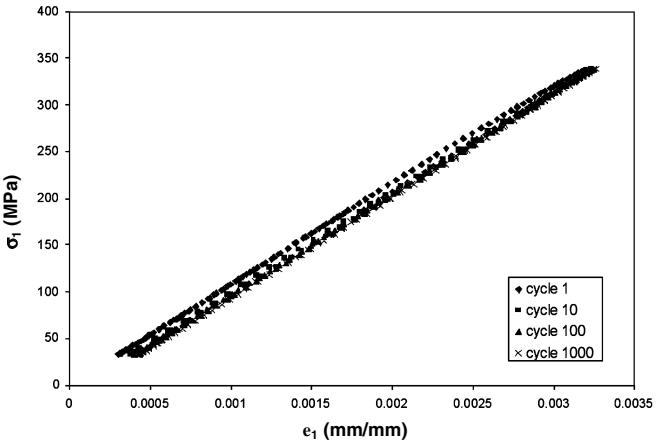

Fig. 5. Stress-strain curve for 10° off-axis graphite BMI in the longitudinal (1) direction. σ_{max}=350 MPa, N_f=1158.

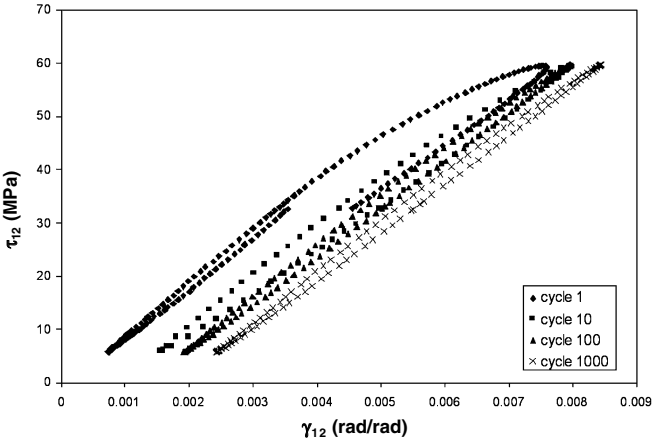

Fig. 7. Stress-strain curve for 10° off-axis graphite BMI in the shear (12) plane. σ_{max}=350 MPa, N_f=1158.

defined strain shifts. For this reason, it was decided that these changes in the shear stress-strain response would be used as the base for expressing macroscopic damage.

Metallographic Examination

Photomicrographs of the surface taken from the acetate tapes showed that longitudinal cracks which propagated along the fibre-matrix interface were dominant throughout the life of the specimens.

The acetate replicas allowed crack damage profile plots to be developed. Figure 8 is representative indicating accumulation of the longitudinal cracks in terms of their number and length over the life of the specimen. Although the replicas were taken from a small portion of the polished area of the specimen surface, they were too large to characterize the length of all cracks within each replica. Accordingly, ten randomly chosen frames were measured using a magnification of 1000×, giving a total area of 80,000 μm^2. This method of crack counting facilitated comparisons to be made between different loading stages and between different specimens.

Transverse matrix and fibre cracks were also monitored. However, the longitudinal cracks were of main interest because they were numerically dominant and controlled the final failure.

Figure 8 shows that initially a large number of small longitudinal cracks (<10 μm) formed. New cracks continued to form until saturation occurred at approximately 10% life. Subsequently, damage appeared to remain relatively constant indicating a change from crack initiation to growth including coalescence. Since only the surface cracks were monitored, it was possible that further damage was accumulating as evidenced by the cracks growing deeper and thereby increasing their aspect ratios.

Considering uniform crack distribution, two separate stages of surface crack development became apparent. In

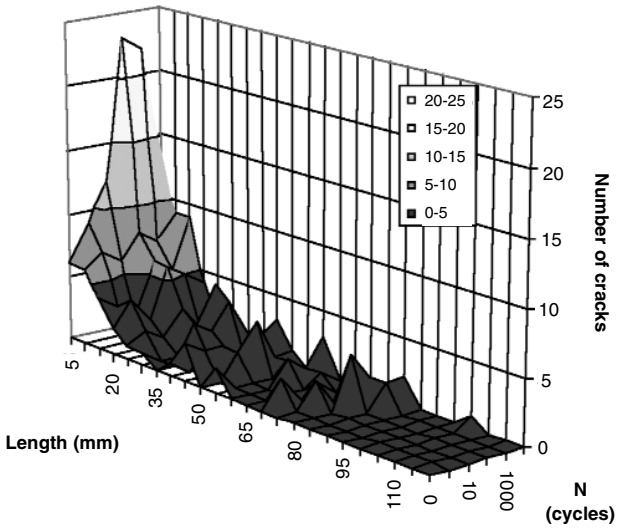

Fig. 8. Variation of debond crack number and length with increasing number of cycles. N_f=1158 cycles. The number of cracks was normalized using the replicated area of 80,000 μm^2.

stage I, crack nucleation occurred with little growth in the bulk material. Figure 9 shows this to effect. A large number of cracks formed on the first cycle and their number increased twofold within the first 10% life. Their lengths remained relatively constant during this first stage. In stage II, the newly formed cracks gradually became longer with coalescence becoming pronounced for the last part of life. In this case after 1000 cycles (75% life), the average crack length rapidly increased at the expense of the average number of cracks.

In contrast to the static tensile test specimens that displayed strong matrix adherence to the fibres after fracture [15], the fatigued specimens showed only small amounts of matrix material adhering to the fibres. After a large number of cycles, many of the fibres on the fracture surface were bare (Figure 10). It is anticipated that the bare fibres and

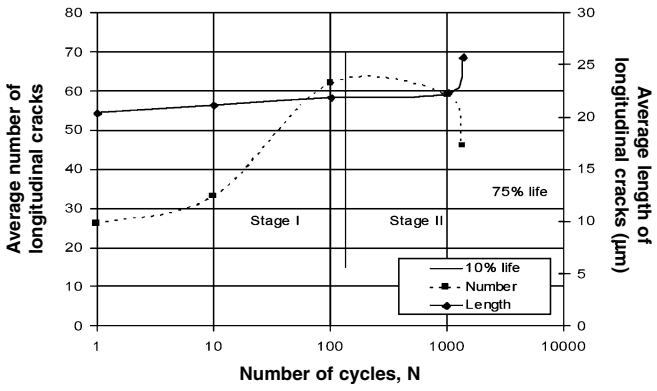

Fig. 9. Variation of average number of longitudinal cracks and average length with increasing number of cycles. N_f=1158 cycles. The crack density was measured in an area of 80,000 μm^2.

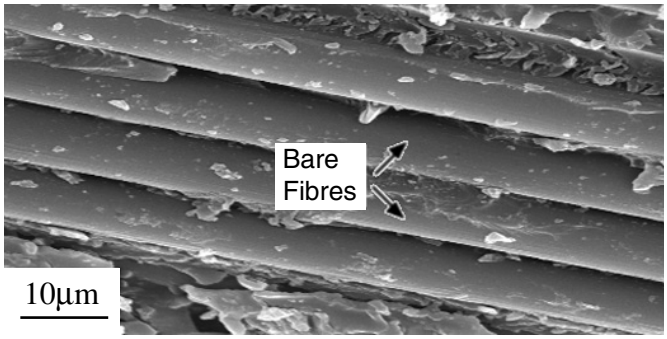

Fig. 10. SEM micrograph of bare fibres on the fracture surface of a 10° off-axis graphite BMI composite.

accompanying matrix debris on the fracture surface resulted from the relative movement of the crack faces during cycling causing wear rather than a poor interfacial bond or one sensitive to cyclic loading. Once small interfacial cracks form, the large cyclic shear stresses can cause relative displacement of the crack faces resulting in the formation of matrix wear debris.

DISCUSSION

The crack growth data given in Figure 8 and Equation 1 were used to define an empirical microscopic damage parameter. In order to relate the number and length of cracks shown in Figures 8 and 9 to the damage parameter given by Equation 1, the cracked area for the dominant damage mechanism must be considered. The majority of the longitudinal cracks were interfacial, either elliptical or cylindrical, depending on their length (Figure 1). Since there was a three-dimensional stress field between the fibres [25], it can be assumed that initially the cracks grew faster in the fibre direction than around the circumference resulting in an elliptical profile. Microscopic observation indicated that small elliptical cracks grew with a constant aspect ratio (a/c=0.33) until their length was 20 μm which was about three times the fibre diameter (7-8 μm). They then changed to cylindrical cracks with projected depths approximately equal to the average fibre diameter; after that, only the length of the crack appeared to increase.

Figure 11 shows this crack based fatigue damage parameter plotted against the normalized number of cycles to failure. A two-stage damage evolution process is seen with the numerous small longitudinal cracks being responsible for stage I, whereas few new cracks and a small change in total cracked area occur during stage II. Although some new cracks form, the overall number decreases due to coalescence.

The macroscopic damage parameter was determined from the stress-strain response using the fatigue modulus, Equation 2. Applying this parameter based on shear modulus degradation, Figure 12 shows the evolution of fatigue damage. During initial cyclic testing, the amount of

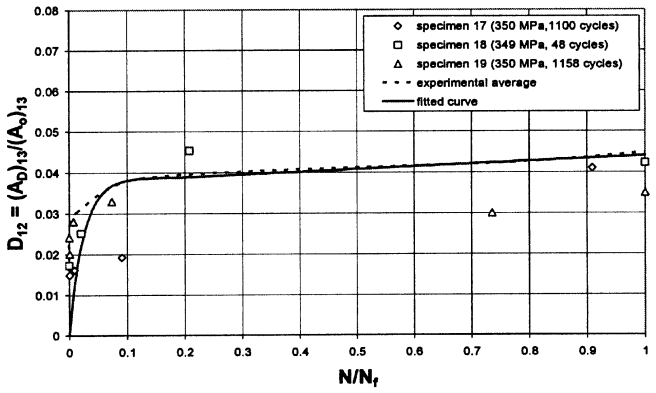

Fig. 11. Variation of longitudinal crack damage with normalized number of cycles to failure.

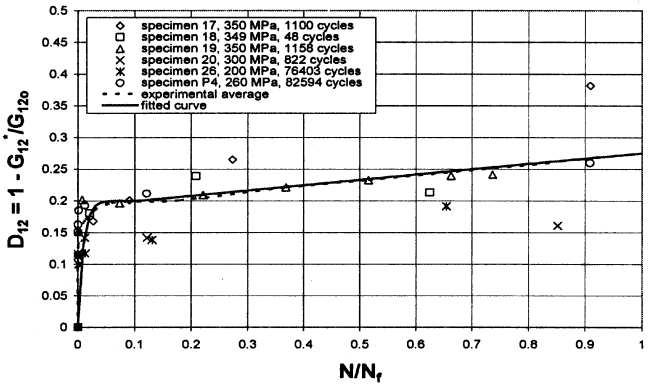

Fig. 12. Variation of shear fatigue damage with normalized number of cycles.

damage increased dramatically, then saturated at about 10% life. After this point, there was little change in the shear modulus. Again, two different stages to the damage process were indicated.

Comparing the two methods of monitoring damage, both indicate a two stage process during the fatigue of the composite. For a particular stress level, the initial crack density and distribution are established within the first few cycles and this appears to determine the eventual life. On saturation and once these cracks have started to coalesce, a general life prediction may be made on the basis that approximately 90% of the life remains after this point. Sorensen and Plumtree [26] and Cain *et al*. [27] demonstrated that this approach can be used successfully to predict the life of off-axis graphite fibre polymer based composites.

The two-stage damage process can be expressed [12] by

$$D_T = D_1'\left\{1-\exp\left[-\frac{N}{\alpha}\right]^{\beta}\right\} + D_2'\left\{1-\left(\frac{N}{N_f}\right)^{\gamma}\right\} \qquad (5)$$

where D_T is the total damage accumulated after N cycles and D'_1 and D'_2 are the amounts of damage at the end of stages I and II, respectively (Figure 13a). The constants α, β and γ depend on the material and the loading conditions. In the present work, accumulation of damage in the second stage is approximately linear; hence, γ may be taken as unity and, accordingly, the second component of Equation 5 becomes linear. This assumption is valid when there is little damage due to fibre fracture which was confirmed by microscopic examination.

Combining the longitudinal crack damage data for all tests carried out on a maximum stress level of 350 MPa, the characteristic expression based on Equation 5 becomes

$$D_T = 0.039\left\{1-\exp\left[-\frac{N}{31.3}\right]^{0.92}\right\} + 0.044\left\{1-\frac{N}{N_f}\right\} \qquad (6)$$

Similarly, by averaging the shear fatigue damage modulus curves for the same maximum stress level, the following characteristic equation is obtained.

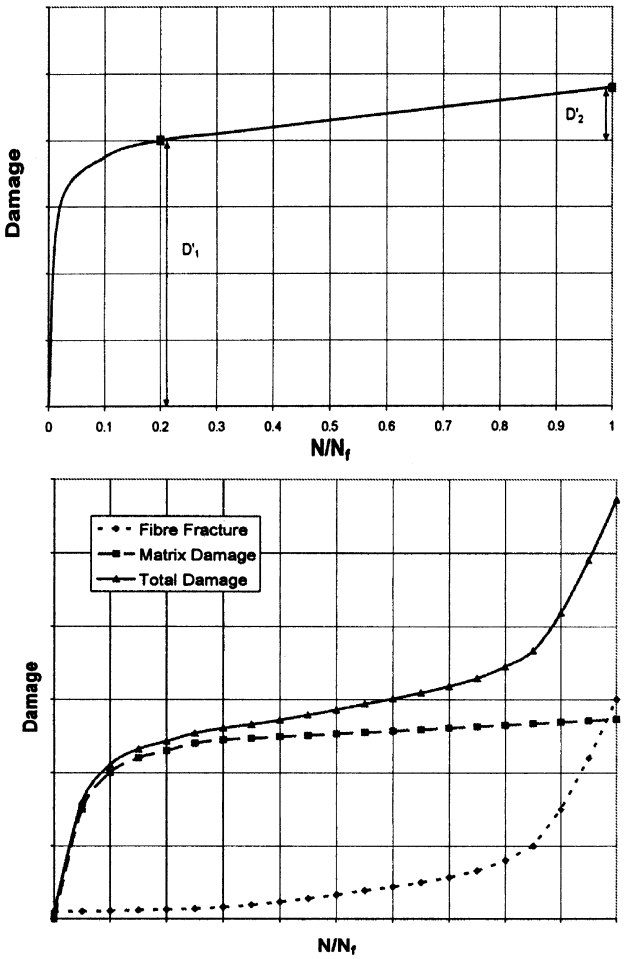

Fig. 13. a) Two-stage damage evolution. Damage variation with increasing normalized cycles. D'_1 and D'_2 are the damage at the end of stage I and II, respectively. b) Damage evolution as a combination of non-progressive damage, that due to fibre fracture, and progressive damage, that due to matrix cracking.

$$D_T = 0.20\left\{1 - \exp\left[-\frac{N}{8.85}\right]^{0.69}\right\} + 0.28\left\{1 - \frac{N}{N_f}\right\} \qquad (7)$$

Although similar in form, these characteristic damage equations yield different quantitative results. This is not unexpected since the shear damage used for Equation 7 is dominated by strain ratcheting that does not directly relate to crack density, although it possibly reflects irreversible matrix damage. Considering the crack-based approach, Equation 6 can be modified to include the effect of stress concentrations at the crack tip which would result in a greater effective cracked area. In doing so, a multiplying factor of about 5 accounts for this difference and is consistent with the stress-strain concentration factors according to Kies [25] and Adams and Doner [28]. The crack-based damage parameter may likely need further revision for it assumes that the crack depth remains constant during stage II. Observations on metallic specimens subjected to cyclic shear tests have shown that although the surface crack length remains relatively constant for a large portion of life, the cracks grow rapidly in depth as fracture becomes imminent [29]. However, Equations 6 and 7 convey the same overall behaviour and depict a similar progression of matrix damage. On considering the two, the parameter based on a fatigue modulus has an advantage since it is more easily monitored without interfering or stopping the test procedure.

CONCLUSIONS

From the analysis of cyclic damage using a microstructural examination and a stress-strain response of an off-axis graphite-BMI composite, several conclusions were made.

1. The evolution of fatigue damage based on a longitudinal crack area showed two stages. There was a period of rapid crack growth during the first 10% of life. This was followed by a period of coalescence where the number of cracks remained relatively constant. During this second stage, dominant shear cracks developed along the fibre-matrix interface eventually causing fracture.
2. Fatigue damage evolution in terms of shear modulus degradation also displayed a two-stage process. Again, damage progressed rapidly during the first 10% of life and once this first stage was completed, a relatively small amount of damage accumulated for the remaining life of the composite.
3. Saturation of both damage parameters after about 10% life indicated that the initial crack pattern and rate of coalescence, eventually forming a dominant fatigue crack, were critical parameters. The crack pattern was established very early during stage I. Approximately half the total lifetime number of cracks formed in the first few cycles and these ultimately dictated the life of the composite.
4. Characteristic damage equations were developed for both crack-based and modulus-based damage parameters. Both successfully described the evolution of damage due to cyclic loading.

ACKNOWLEDGEMENTS

The authors gratefully acknowledge the Institute for Aerospace Studies of the National Research Council of Canada for the manufacture of the composite plates. This research has been funded by the Natural Sciences and Engineering Research Council of Canada.

REFERENCES

1. H.T. Hahn, "Fatigue Behaviour and Life Prediction of Composite Laminates", *ASTM STP 674, Composite Materials: Testing and Design,* 1979, vol. 5, S.W. Tsai, ed., pp. 383-417.
2. A. Rotem, "Fatigue Failure Mechanism of Composite Laminates", *Mechanics of Composite Materials, Recent Advances*, 1983, Z. Hashin and C.T. Herakovich, eds., pp. 421-435.
3. N.V. Akshantala and R.A. Talreja, "Micromechanics Based Model for Predicting Fatigue Life of Composite Laminates", *Materials Science and Engineering,* 2000, vol. A283, pp. 303-313.
4. K. Schulte, "Damage Monitoring in Polymer Matrix Structures", *Journal de Physique*, 1993, vol. IV, pp. 1629-1636.
5. K.L. Reifsnider, "Damage and Damage Mechanics", *Composite Materials Series, Fatigue of Composite Materials*, 1991, vol. 4, K.L. Reifsnider, ed., pp. 11-77.
6. K. Schulte, "Stiffness Reduction and Development of Longitudinal Cracks During Fatigue Loading of Composite Laminates", *Mechanical Characterization of Load Bearing Fibre Laminates,* 1985, A.H. Cardon and G. Verchery, eds., Elsevier. pp. 36-54.
7. R.S. Jamison, K. Schulte, K.L. Reifsnider, and W.W. Stinchcomb, "Characterization and Analysis of Damage Mechanisms in Tension-Tension Fatigue of Graphite Epoxy Laminates", *ASTM STP 836, Effects of Defects in Composite Materials,* 1984, D.J. Wilkens, ed., pp. 21-55.
8. K.L. Reifsnider, E.G. Henneke, W.W. Stinchcomb and J.C. Duke, "Damage Mechanics and NDE of Composite Laminates". *Mechanics of Composite Materials, Recent Advances*, 1983, Z. Hashin and C.T. Herakovich, eds., Permagon Press, U.S.A., pp. 399-420.
9. A.L. Highsmith and K.L. Reifsnider, "Stiffness Reduction Mechanisms in Composite Laminates", *ASTM STP 775, Damage in Composite Materials*, 1982, K.L. Reifsnider, ed., pp. 103-117.
10. N.V. Akshantala and R. Talreja, "A Mechanistic Model for Fatigue Damage Evolution in Composite Laminates", *Mechanics of Materials*, 1998, vol. 29, pp. 123-140.
11. R. Talreja, *Fatigue of Composite Materials*, 1987, Technomic Publishing Company, U.S.A.
12. A. Plumtree and G. Shen, "Prediction of Fatigue Damage Development in Unidirectional Long Fibre Composites", *Polymers and Polymer Composites*, 1994, vol. 2, pp. 83-90.
13. S.M. Jessen and A. Plumtree, "Fatigue Damage Accumulation in Glass/Polyester Pultruded Rods", *Composites*, 1988, vol. 20, pp. 559-567.
14. L.M. Kachanov, "On Creep Rupture Time", *Izv. Acad. Nauk SSSR, Otd. Techn. Nau,* 1958, vol. 8, pp. 26-31.
15. K. Cain, G. Glinka and A. Plumtree, "Damage Evolution in an Off-Axis Unidirectional Graphite Bismaleimide Composite Loaded in Tension", *Composites A*, 2002, vol. 34, pp. 987-993.
16. R.S. Jamison, K. Schulte, K.L. Reifsnider and W.W. Stinchcomb, "Characterization and Analysis of Damage Mechanisms in Tension-Tension Fatigue of Graphite Epoxy Laminates", *ASTM STP 836, Effects of Defects in Composite Materials*, 1984, pp. 21-55.
17. K. Schulte, "Stiffness Reduction and Development of Longitudinal Cracks During Fatigue Loading of Composite Laminates", *Mechanical Characterization of Load Bearing Fibre Laminates,* 1985, A.H. Cardon and G. Verchery, eds., Elsevier Applied Science Publishers, pp. 36-54.
18. K. Schulte, "Damage Monitoring in Polymer Matrix Structures", *Journal de Physique*, 1993, vol. IV, pp. 1629-1636.

19. W. Hwang and K.S. Han, "Cumulative Damage Models and Multi-Stress Fatigue Life Prediction", *ASTM STP 1012, Composite Materials: Fatigue and Fracture*, 1989, vol. 2, pp. 87-102.
20. A. Plumtree and L. Shi, "Fatigue of Unidirectional Carbon Fibre Reinforced Epoxy", *Proceedings of the 7th International Conference on Fibre Reinforced Composites,* April, 1998, 498-505, Newcastle upon Tyne, U.K., pp.15-17.
21. S.S. Wang and Chim, "Fatigue Damage and Degradation in Random Short-Fibre SMC Composite", *Journal of Composite Materials,* 1983, vol. 17, pp. 114-34.
22. G. Shen, *Fatigue Life Prediction of Composites Based on Microstress Analysis,* 1993, Ph.D. Thesis, University of Waterloo, Ontario.
23. S. Lee, R.F. Scott, P.C. Gaudert, W.H. Ubbink and C. Poon, "Mechanical Testing of Toughened Resin Composite Materials", *Composites*, 1988, vol. 19, pp. 300-310.
24. J. Awerbuch and H.T. Hahn, "Off-Axis Fatigue of a Graphite/Epoxy Composite", *ASTM STP 569, Fatigue of Composite Materials*, 1975, pp. 171-188.
25. J.A. Kies, *Maximum Strains in the Resin of Fiberglass Composites,* 1962, US Naval Research Laboratory Report NRL 5752.
26. L.K. Sorensen and A. Plumtree, "Assessment of Damage in a Unidirectional Off-Axis Carbon-Epoxy Composite under Cyclic Loading." *ASTM STP 1436, Composite Materials: Testing and Design*, 2003, vol. 14, C.E. Bakis ed., pp. 336-348.
27. K.J. Cain, G. Glinka and A. Plumtree, "Fatigue Damage Evolution of an Off-Axis Unidirectional Carbon Bismaleimide Composite", *Proceedings of CANCOM,* August 2003, Ottawa, Canada. Paper 83, pp. 1-10.
28. D.F. Adams and D.R. Doner, "Longitudinal Shear Loading of a Unidirectional Composite", *Journal of Composite Materials,* 1967, vol. 1, pp. 4-17.
29. A. Varvani-Farahani, "Biaxial Fatigue Crack Growth and Crack Closure Under Constant Amplitude and Periodic Compressive Overload Histories in 1045 Steellocklin", Ph.D. Thesis, 2001, Mechanical Engineering University of Waterloo, Canada.